*American Mineralogist, Volume 108, pages 2234–2243, 2023*

# $S_2^-$ and $S_3^-$ radicals and the $S_4^{2-}$ polysulfide ion in lazurite, haüyne, and synthetic ultramarine blue revealed by resonance Raman spectroscopy

**Stefan Farsang[1,*], Razvan Caracas[2,3], Takuji B.M. Adachi[4], Cédric Schnyder[5], and Zoltán Zajacz[1]**

[1]Department of Earth Sciences, University of Geneva, Rue des Maraîchers 13, 1205 Geneva, Switzerland
[2]Institut de Physique du Globe de Paris, Université de Paris Cité, CNRS, Paris, France
[3]The Center for Earth Evolution and Dynamics (CEED), University of Oslo, 0371 Oslo, Norway
[4]Department of Physical Chemistry, University of Geneva, Quai Ernest Ansermet 30, 1211 Geneva, Switzerland
[5]Natural History Museum of Geneva, Route de Malagnou 1, 1208 Geneva, Switzerland

## Abstract

Taking advantage of the Raman resonance effect, we employed 405 and 532 nm excitations to (1) identify sulfur species present in lazurite, haüyne, and synthetic ultramarine blue pigments and (2) investigate the enigmatic ~485 $cm^{-1}$ band found previously in Raman spectra of lazurite and haüyne collected with 458 nm excitation. In spectra of lazurite and haüyne, bands of the sulfate ion and $S_2^-$ and $S_3^-$ radicals can be seen. Spectra collected using 405 nm excitation show the enhancement of the intensity of $\nu_1(S_2^-)$ band and its $n\nu_1$ ($n \leq 7$) progression. Spectra collected using 532 nm incident light show the enhancement of intensity of $\nu_1(S_3^-)$, $\nu_2(S_3^-)$, and $\nu_3(S_3^-)$ bands and the $n\nu_1$ ($n \leq 9$) and $\nu_2 + n\nu_1$ progressions of the $\nu_1(S_3^-)$ band. In spectra collected with 405 nm excitation, we also found features that we ascribe to the $S_4^{2-}$ polysulfide ion. These include the $\nu_1$ symmetric S-S stretching band at ~481 $cm^{-1}$, the $\nu_2$ symmetric S-S stretching band at ~443 $cm^{-1}$ (only present in spectra of some lazurite samples), the $\nu_3$ symmetric S-S bending at 223 $cm^{-1}$ and the $n\nu_1$ ($n \leq 5$) and $n\nu_1+\nu_3$ progressions of the $\nu_1(S_4^{2-})$ band. We observed that under laser illumination, the $S_4^{2-}$ polysulfide ion rapidly decomposes into two $S_2^-$ radicals in lazurite while it remains stable in haüyne. In spectra of synthetic ultramarine blue pigments, only features of $S_2^-$ and $S_3^-$ radicals were observed. Finally, we verified the identity of the radical and polysulfide ions with ab initio molecular dynamics calculations. We conclude that Raman resonance spectroscopy is a powerful qualitative method to detect polysulfide and sulfur radical species with concentrations below the detection limit of conventional analytical techniques. Owing to the high stability of $S_4^{2-}$ in haüyne, this mineral structure appears promising as a host material for $S_4^{2-}$ entrapment, making it potentially useful for applications in optoelectronics.

**Keywords:** Haüyne, lapis lazuli, lazurite, molecular dynamics, resonance Raman spectroscopy, sodalite group, sulfur radical, ultramarine blue pigment

## Introduction

Sodalite group minerals, including lazurite $Na_7Ca(Al_6Si_6O_{24})(SO_4)^{2-}(S_3)^{-}\cdot H_2O$ (Sapozhnikov et al. 2021) and haüyne $Na_{4.5}Ca_2K[Al_6Si_6O_{24}](SO_4)_{1.5}(OH)_{0.5}$ (Hassan and Grundy 1991), are members of the feldspathoid family. Feldspathoids share an aluminosilicate framework consisting of six-membered rings of Si- and Al-centered tetrahedra. The sodalite group is characterized by a sodalite-type (ABC) stacking sequence of aluminosilicate layers and the presence of sodalite (β) cages that can accommodate various cations, anions, and neutral molecules (Sapozhnikov et al. 2021), including several sulfur species (Table 1). Of these, the $S_3^-$ and $S_2^-$ radicals deserve special attention for two reasons. First, the sodalite cage is one of the few environments in which these sulfur species can be stabilized at ambient temperature. In geologic fluids, for instance, sulfur radicals become stable only around 200 °C (Pokrovski and Dubrovinsky 2011). Second, sulfur radicals are chromophores. Whereas the $S_3^-$ radical is a blue chromophore (Chivers 1974) that made lapis lazuli a highly prized gemstone of the Sumerian and Egyptian antiquity (Gaetani et al. 2004), and the ultramarine blue made from lazurite a desired pigment in both Asia and Europe since the 7th–8th century CE (Gettens 1938; Gaetani et al. 2004), the $S_2^-$ radical is a yellow chromophore and the increasing $S_2^-/S_3^-$ ratio was found to be responsible for greenish shades and eventually green color of ultramarine pigments (Clark and Cobbold 1978; Reinen and Lindner 1999). Just like lazurite, blue crystals of haüyne also owe their color to $S_3^-$ radicals (Caggiani et al. 2022).

Given that the identification of sulfur radicals may be hindered by their low concentrations, we decided to employ Raman spectroscopy in the search for sulfur-bearing species and take advantage of the Raman resonance effect shown by sulfur radicals (Clark and Franks 1975; Clark and Cobbold 1978; Clark and Dines 1986; Picquenard et al. 1993). Furthermore, we investigated the enigmatic ~485 $cm^{-1}$ band found previously in Raman spectra of lazurite and haüyne collected with a 458 nm excitation, which was invisible in spectra collected with a 532 nm excitation and was suggested to be related to the $\nu_1$ band of $S_2^-$ radical (Caggiani et al. 2014).

## Methods

### Samples

Raman spectra were collected on naturally occurring lazurite and haüyne samples provided by the Natural History Museum, Geneva, Switzerland, and

* E-mail: stefan.farsang@unige.ch. Orcid 0000-0002-4918-5566


0003-004X/23/0012–2234$05.00/DOI: https://doi.org/10.2138/am-2022-8655

**Table 1.** Sulfur species in lazurite and haüyne

| Locality | Sulfur species | Analytical method | Reference |
|---|---|---|---|
| | **Lazurite** | | |
| Afghanistan, Baffin Island, Nunavut, Canada | Sulfate $SO_4^{2-}$, Monosulfide $S^{2-}$ | XRD | Hassan et al. (1985) |
| Pamir, Tajikistan | Sulfate $SO_4^{2-}$, $S_3^-$ radical, $S_2^-$ radical | Raman, UV-Vis, IR, EPR | Ostroumov et al. (2002) |
| Afghanistan, Baffin Island, Nunavut, Canada | Sulfate $SO_4^{2-}$ (ma), Monosulfide $S^{2-}$ bound to Na (mi), Elemental sulfur S (mi), Polysulfide (mi) | XANES, XPS | Fleet et al. (2005) |
| Malo-Bystrinskoe Deposit, Lake Baikal Region, Russia | Sulfate $SO_4^{2-}$ (ma), Polysulfide (ma), Sulfite $SO_3$ (mi), Monosulfide $S^{2-}$ (mi), Thiosulfate $S_2O_3$ (mi), Elemental sulfur S (mi) | XANES, XPS | Tauson et al. (2012) |
| Badakhshan, Afghanistan | Sulfate $SO_4^{2-}$, $S_3^-$ radical, $S_2^-$ radical | Raman | Caggiani et al. (2014) |
| Many localities | Sulfate $SO_4^{2-}$, $S_3^-$ and/or $S_2^-$ radical, $S_2^-$ radical | XANES | Gambardella et al. (2016) |
| Malo-Bystrinskoe Deposit, Lake Baikal Region, Russia | Sulfate $SO_4^{2-}$ (ma), $S_3^-$ radical(ma), Monosulfide $S^{2-}$ (mi, not detected directly) | IR, Raman, EPR, XPS | Sapozhnikov et al. (2021) |
| | **Haüyne** | | |
| Sacrafano, Italy | Sulfate $SO_4^{2-}$ | XRD | Hassan and Grundy (1991) |
| Toppo, San Paolo, Italy Near Mount Vulture volcano, Italy | Sulfate $SO_4^{2-}$, $S_3^-$ radical, $S_2^-$ radical | Raman | Caggiani et al. (2014) |
| Toppo, San Paolo, Italy Melfi, Italy | Sulfate $SO_4^{2-}$, $S_3^-$ radical, $S_2^-$ radical | Raman | Caggiani et al. (2022) |

*Notes*: ma = major phase; mi = minor phase; EPR = electron paramagnetic resonance spectroscopy; IR = Infrared spectroscopy; UV-Vis = Ultraviolet-visible spectroscopy; XANES = X-ray absorption near-edge structure; XPS = X-ray photoelectron spectroscopy; XRD = X-ray diffraction.

ultramarine blue pigments purchased from Kremer Pigmente, Germany (see the raw spectra data in the Online Materials[1]). The origin of lazurites is as follows: specimen number 003.084 Baikal, Russia; 376.002 Tunnel Mt Cenis, Savoie, France; 397.041 Badakhstan, Kabul, Afghanistan; 425.086 Brazil; and 431.065 Sierra d'Ovalle, Coquimbo, Chile. The origin of haüynes is as follows: 333.049 Mount Vesuvius, Italy, and 332.018 Laachersee, Eifel, Germany. The pigments analyzed were: 45000 Ultramarine blue, very dark; 45010 Ultramarine blue, dark; 45020 Ultramarine blue, reddish; 45030 Ultramarine blue, greenish extra; 45040 Ultramarine blue, greenish light; and 45080 Ultramarine blue, light.

## Diffuse reflectance spectroscopy

Diffuse reflectance spectra were collected using a UV-visible spectrometer (V-670, JASCO) coupled with an integrating sphere accessory (ARSN-733, JASCO) at the Department of Physical Chemistry, University of Geneva (see the raw spectra data in the Online Materials[1]). Each mineral powder sample was mixed with KBr (ca. 1 wt% of a sample in KBr) for the preparation of a 13 mm circular pellet (a Specac hydraulic press was used). The pellet was then mounted on the sample holder of the integrated sphere, and the diffuse reflectance spectra were measured. A blank KBr pellet was used for obtaining the background spectrum. The measured reflectance ($R$) was converted to absorbance ($A$) by calculating $A = -\log R$.

## Raman spectroscopy

Raman spectra collected with 405 and 532 nm excitations were acquired using a confocal LabRAM HR Evolution (HORIBA Scientific) Raman spectrometer with 800 mm focal length at the Department of Earth Sciences, University of Geneva. To emphasize the enhancement of $S_2^-$ and $S_3^-$ bands due to the Raman resonance effect, spectra were also collected with a 785 nm excitation using a Renishaw inVia Raman spectrometer with 250 mm focal length at the Natural History Museum of Geneva. However, the interpretation of previously observed spectral features of lazurite in spectra collected with a 785 nm excitation (e.g., González-Cabrera et al. 2022) is beyond the scope of the current study. Both spectrometers were calibrated using the 521 $cm^{-1}$ line of silicon.

The LabRAM spectrometer was equipped with a liquid nitrogen cooled, back-illuminated Symphony II CCD detector (1024 × 256 pixel) and an Olympus BXFM microscope with a motorized XYZ sample stage. The spectral resolution was ~0.5 $cm^{-1}$. A grating of 1800 lines/mm and a confocal pinhole of 100 µm were employed. A TopMode 405 laser source (Toptica Photonics) with a wavelength of 405 nm and a Torus 532 laser source (Laser Quantum) with a wavelength of 532 nm were used for excitation. The spectra were acquired in backscattering geometry using either an Olympus MPlan N 100× objective with the numerical aperture of 0.90 and a working distance of 0.21 mm (for lazurites and pigments) or an Olympus LMPlanFL N 50× long working distance objective with a numerical aperture of 0.50 and a working distance of 10.6 mm (for haüynes).

The Renishaw spectrometer was equipped with a Peltier cooled CCD detector (400 × 576 pixel) and a DM Leica 2500 microscope with a motorized XYZ sample stage. The spectral resolution was ~1.5 $cm^{-1}$. A grating of 1200 lines/mm and a slit of 65 µm were employed. A HPNIR785 diode laser source (Renishaw) with a wavelength of 785 nm was used for excitation. The spectra were acquired in backscattering geometry using a Leica 50× long working distance objective with the numerical aperture of 0.55 and the working distance of 8 mm.

For each spectrum collected with the 405 and 532 nm lasers, three accumulations of 10 s each were taken in multiple spectral windows resulting in a final range of 150–5000 $cm^{-1}$. In addition, spectra with 10 accumulations of 10 s each were taken in the spectral window of 400–700 $cm^{-1}$. To prevent the saturation of the CCD detector while collecting spectra of lazurites and to prevent the burning of pigments, a power filter of 10% was also applied for these measurements, reducing the maximum power of ~30 mW measured at the sample to ~3 mW.

For each spectrum collected with the 785 nm laser, 10 accumulations of 10 s each were taken in the spectral window of 400–1200 $cm^{-1}$. To prevent the saturation of the CCD detector, power filters of 1, 5, or 10% were applied for the measurement of lazurites and haüynes, and to prevent the burning of samples, a power filter of 0.1% was applied for the measurement of pigments, significantly reducing the maximum power of ~300 mW measured at the sample.

## Ab initio molecular dynamics

Molecular dynamics simulations were performed using the VASP package (Kresse and Hafner 1993; Kresse and Joubert 1999). The interatomic forces were computed using the planar augmented wave function method (Blöchl 1994). The generalized gradient approximation (Perdew et al. 1996) was used to describe the exchange correlation term of the energy. The electronic density and wave functions were computed using the sampling of the reciprocal space in the Γ point. The simulations were run for at least 30 picoseconds with a time step of 1 femtosecond.

The analysis of the simulations was completed using the UMD package (Caracas et al. 2021a, 2021b). The geometry of the S-S bonds was monitored by computing the pair distribution functions (PDFs). The first minimum of the PDFs yields the maximum bond distance and in a fluid description corresponds to the radius of the first coordination sphere. This distance was used to assess the speciation within the radical and polysulfide ions. The vibrational spectra were obtained as the Fourier transform of the self-correlation function of the atomic velocities.

# Results and discussion

Raman resonance means that when a molecule is excited with a laser with a frequency close to the maximum of an allowed electronic transition, the Raman spectra are characterized

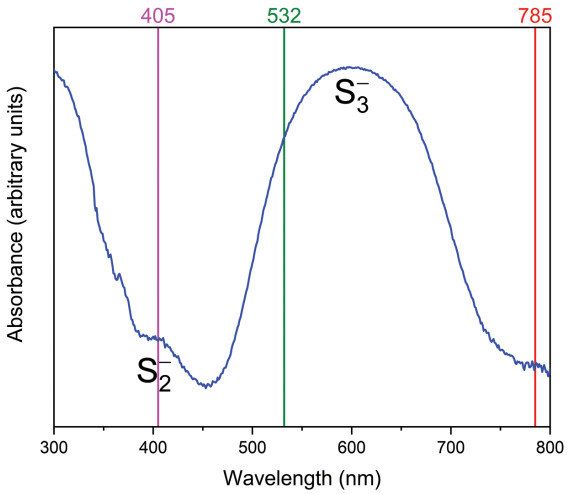


**Figure 1.** Diffuse reflectance spectrum of the NHMG425.086 lazurite sample from Brazil showing absorption bands of $S_2^-$ and $S_3^-$ radicals. The 405, 532, and 785 nm excitation lines used in this study are also shown.

by an enhancement in the intensity of a totally symmetric fundamental of the scattering molecule and by high-intensity overtone progressions in this fundamental (Holzer et al. 1970; Nafie et al. 1971; Clark and Franks 1975). Whereas the $S_3^-$ radical shows a broad absorption band with a maximum around 610–620 nm due to the $X^2B_1 \rightarrow C^2A_2$ transition (Chivers and Drummond 1972; Seel et al. 1977; Clark and Cobbold 1978; Reinen and Lindner 1999; Linguerri et al. 2008; Shnitko et al. 2008), the $S_2^-$ radical shows an absorption band with a maximum around 390–400 nm due to the $^2\Pi_g \rightarrow {}^2\Pi_u$ transition (Fig. 1) (Holzer et al. 1969; Clark and Cobbold 1978). Therefore, we employed 405 nm excitation that lies inside the absorbance band of the $S_2^-$ radical, 532 nm excitation that lies inside the absorbance band of the $S_3^-$ radical, and 785 nm excitation that lies outside the absorbance bands of either radical (Fig. 1) to collect Raman spectra of five lazurites, two haüynes, and six synthetic ultramarine blue pigments to identify the sulfur species present in each (see Online Materials[1]). Representative spectra of these are shown in Figures 2, 3, and 4, respectively. In the following section, the observed bands of sulfur species are discussed.

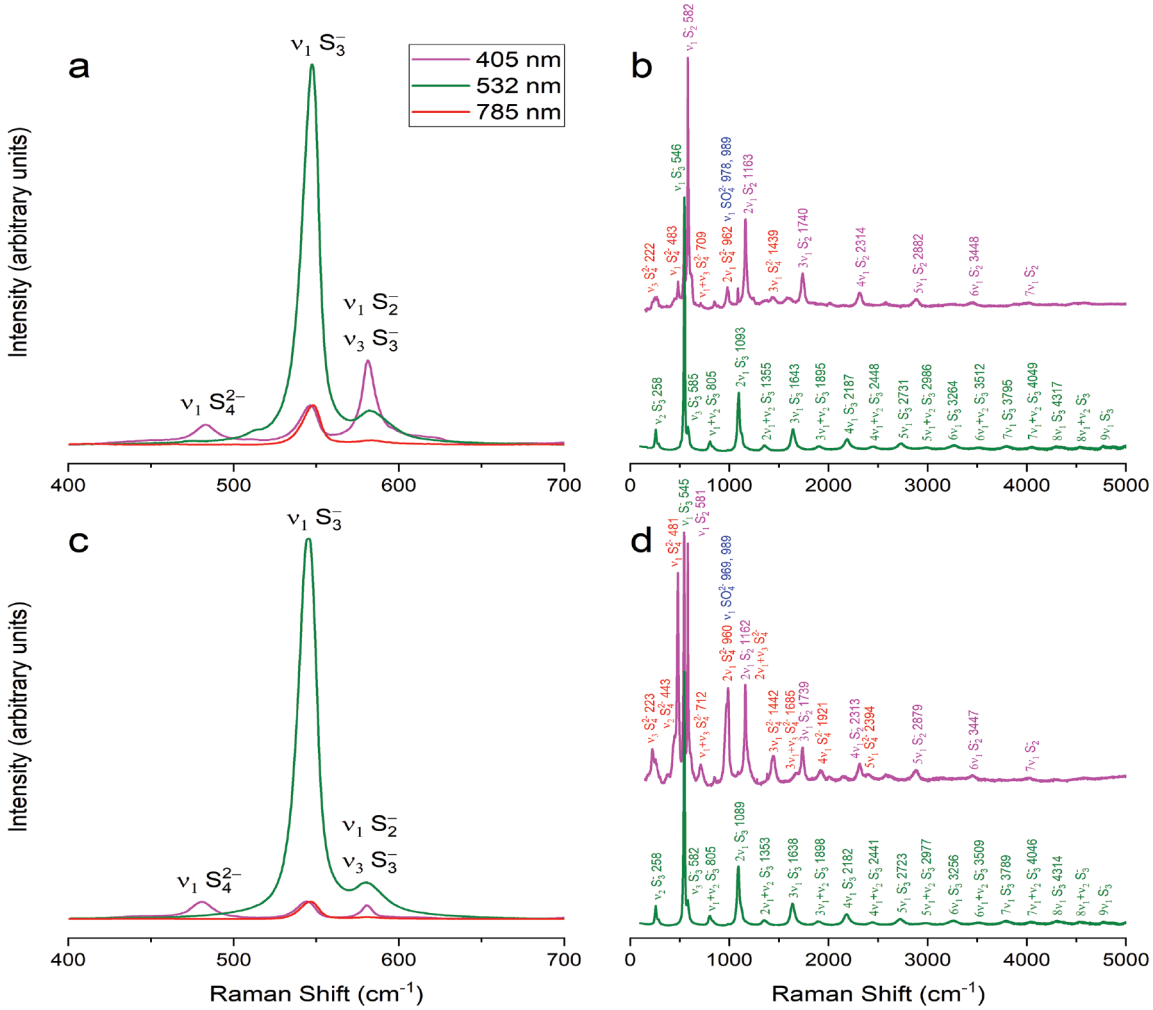


**Figure 2.** Raman spectra of lazurite samples collected with different excitations: (**a** and **b**) spectra of the NHMG003.084 sample from Baikal, Russia; (**c** and **d**) spectra of the NHMG425.086 sample from Brazil. In **b** and **d**, spectra collected with the 405 nm excitation were vertically exaggerated and offset relative to the 532 nm spectra.

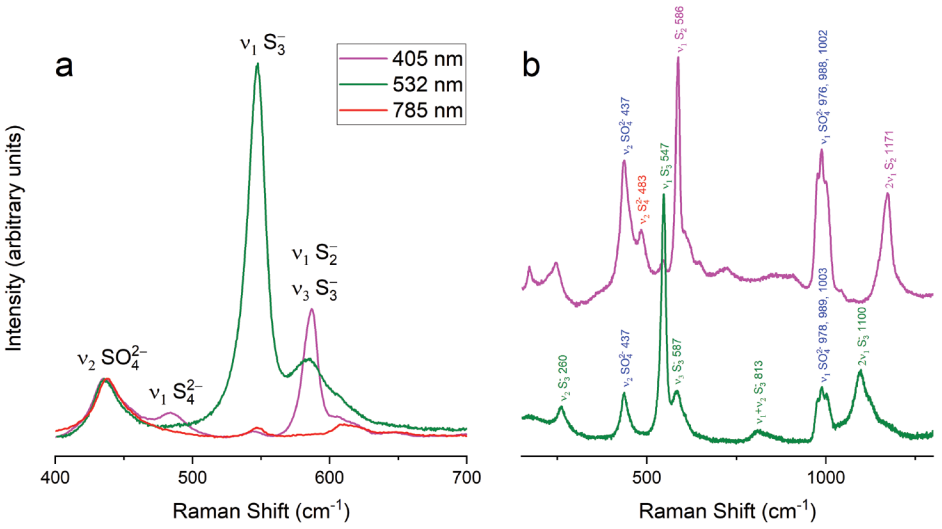


► **Figure 3.** Raman spectra of the NHMG333.049 haüyne sample from Mount Vesuvius, Italy, collected with different excitations. In **b**, the spectrum collected with the 405 nm excitation was vertically exaggerated and offset relative to the 532 nm spectrum.

### Sulfate bands

The $\nu_1(SO_4^{2-})$ bands in the 976–1003 cm$^{-1}$ region, corresponding to the S-O stretching mode (Choi and Lockwood 1989), are visible in most lazurite and haüyne spectra (Figs. 2 and 3), whereas the $\nu_2(SO_4^{2-})$ band at 437 cm$^{-1}$, corresponding to the S-O bending mode (Choi and Lockwood 1989) is only visible in the spectra of haüyne (Fig. 3). In haüyne spectra, up to three bands appear in the sulfate region, likely representing different coordination environments in the sodalite (β) cages. In a recent study, five bands related to the silicate and sulfate groups have been documented in the 950–1030 cm$^{-1}$ spectral region in haüyne originating from the Mount Vulture area in Italy (Caggiani et al. 2022). Sulfate bands are absent in the spectra of ultramarine blues.

### $S_3^-$ bands

The $\nu_1(S_3^-)$ band at ~546 cm$^{-1}$, corresponding to the symmetric S-S stretching mode (Holzer et al. 1969; Chivers and Drummond 1972; Clark and Franks 1975), is visible in all lazurite, haüyne, and ultramarine blue spectra. Given that the 532 nm excitation line lies inside the absorbance band of the $S_3^-$ radical (Fig. 1), spectra collected with the 532 nm excitation show a strong enhancement of the intensity of the $\nu_1(S_3^-)$ band, the $\nu_2(S_3^-)$ band at ~258 cm$^{-1}$, corresponding to the symmetric S-S bending mode (Chivers and Drummond 1972; Clark and Franks 1975), and the $\nu_3(S_3^-)$ band at ~582 cm$^{-1}$, corresponding to the antisymmetric S-S stretching mode (Figs. 2, 3, and 4; Table 2) (Ledé et al. 2007). The 532 nm spectra also show $n\nu_1$ and $\nu_2+n\nu_1$ progressions of the $\nu_1(S_3^-)$ band (Figs. 2, 3, and 4; Table 2).

### $S_2^-$ bands

The position of the $\nu_1(S_2^-)$ band, corresponding to the symmetric S-S stretching mode (Holzer et al. 1969; Clark and Franks 1975), coincides with that of the $\nu_3(S_3^-)$ band (Ledé et al. 2007). Given that the concentration of $S_3^-$ in the studied materials is high enough that its spectral features are visible even in the non-resonant Raman spectra (i.e., those collected with 405 and 785 nm excitations), a small portion of the ~582 cm$^{-1}$ spectral feature in spectra collected with the 405 nm excitation, correspond to the $\nu_3(S_3^-)$ band. The dominant contribution of the

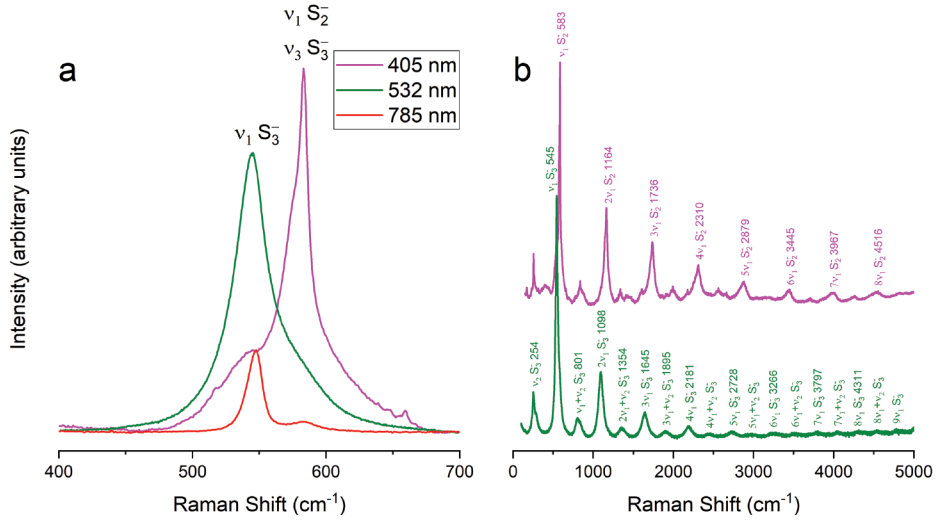


► **Figure 4.** Raman spectra of the "45000 Ultramarine blue, very dark" pigment collected with different excitations. In **b**, the spectrum collected with the 405 nm excitation was vertically exaggerated and offset relative to the 532 nm spectrum.

**TABLE 2.** Observed vibrational frequencies of $S_2^-$ and $S_3^-$ radicals and the $S_4^{2-}$ polysulfide ions in lazurite, haüyne, and ultramarine blue

| | Sample | | | | | | | | | | | | |
|---|---|---|---|---|---|---|---|---|---|---|---|---|---|
| | Lazurite (Russia) | | | Lazurite (Brazil) | | | Haüyne (Italy) | | | Synthetic ultramarine blue | | | Reference for assignment |
| Laser wavelength (nm) | 405 | 532 | 785 | 405 | 532 | 785 | 405 | 532 | 785 | 405 | 532 | 785 | |
| Vibrational mode | | | | | | $S_2^-$ | | | | | | | |
| $\nu_1$ symmetric S-S stretching | 582 | | | 581 | | | 586 | | | 583 | | | Holzer et al. (1969) |
| $2\nu_1$ overtone | 1163 | | | 1162 | | | 1171 | | | 1164 | | | Holzer et al. (1969) |
| $3\nu_1$ overtone | 1740 | | | 1739 | | | | | | 1736 | | | Holzer et al. (1969) |
| $4\nu_1$ overtone | 2314 | | | 2313 | | | | | | 2310 | | | Clark and Franks (1975) |
| $5\nu_1$ overtone | 2882 | | | 2879 | | | | | | 2879 | | | |
| $6\nu_1$ overtone | 3448 | | | 3447 | | | | | | 3445 | | | |
| $7\nu_1$ overtone | | | | | | | | | | 3967 | | | |
| $8\nu_1$ overtone | | | | | | | | | | 4516 | | | |
| | | | | | | $S_3^-$ | | | | | | | |
| $\nu_1$ symmetric S-S stretching | 546 | 546 | 546 | 545 | 545 | 545 | 547 | 547 | 547 | 545 | 545 | 545 | Holzer et al. (1969) |
| $2\nu_1$ overtone | | 1093 | | | 1089 | | | 1100 | | | 1098 | | Holzer et al. (1969) |
| $3\nu_1$ overtone | | 1643 | | | 1638 | | | | | | 1645 | | Holzer et al. (1969) |
| $4\nu_1$ overtone | | 2187 | | | 2182 | | | | | | 2181 | | Holzer et al. (1969) |
| $5\nu_1$ overtone | | 2731 | | | 2723 | | | | | | 2728 | | Holzer et al. (1969) |
| $6\nu_1$ overtone | | 3264 | | | 3256 | | | | | | 3266 | | Holzer et al. (1969) |
| $7\nu_1$ overtone | | 3795 | | | 3789 | | | | | | 3797 | | |
| $8\nu_1$ overtone | | 4317 | | | 4314 | | | | | | 4311 | | |
| $\nu_2$ symmetric S-S bending | | 258 | | | 258 | | | 260 | | | 254 | | Chivers and Drummond (1972) |
| $\nu_1+\nu_2$ overtone | | 805 | | | 805 | | | 813 | | | 801 | | Clark and Franks (1975) |
| $2\nu_1+\nu_2$ overtone | | 1355 | | | 1353 | | | | | | 1354 | | Clark and Franks (1975) |
| $3\nu_1+\nu_2$ overtone | | 1895 | | | 1898 | | | | | | 1895 | | Clark and Franks (1975) |
| $4\nu_1+\nu_2$ overtone | | 2448 | | | 2441 | | | | | | | | |
| $5\nu_1+\nu_2$ overtone | | 2986 | | | 2977 | | | | | | | | |
| $6\nu_1+\nu_2$ overtone | | 3512 | | | 3509 | | | | | | | | |
| $7\nu_1+\nu_2$ overtone | | 4049 | | | 4046 | | | | | | | | |
| $\nu_3$ antisymmetric S-S stretching | | 585 | | | 582 | | | 587 | | | | | Ledé et al. (2007) |
| | | | | | | $S_4^{2-}$ | | | | | | | |
| $\nu_1$ symmetric $S_{central}$–$S_{terminal}$ stretching | 483 | | | 481 | | | 483 | | | | | | Janz et al. (1976) |
| $2\nu_1$ overtone | 962 | | | 960 | | | | | | | | | |
| $3\nu_1$ overtone | 1439 | | | 1442 | | | | | | | | | |
| $4\nu_1$ overtone | | | | 1921 | | | | | | | | | |
| $5\nu_1$ overtone | | | | 2394 | | | | | | | | | |
| $\nu_2$ symmetric $S_{central}$–$S_{central}$ stretching | | | | 443 | | | | | | | | | Janz et al. (1976) |
| $\nu_3$ symmetric S-S bending | 222 | | | 223 | | | | | | | | | Janz et al. (1976) |
| $\nu_1+\nu_3$ overtone | 709 | | | 712 | | | | | | | | | |
| $3\nu_1+\nu_3$ overtone | | | | 1685 | | | | | | | | | |

~582 $cm^{-1}$ spectral feature is the $\nu_1(S_2^-)$ band because the 405 nm excitation line lies inside the absorbance band of the $S_2^-$ radical. The 405 nm spectra of lazurites, haüynes, and ultramarine blues indeed show a greatly enhanced $\nu_1(S_2^-)$ band and its $n\nu_1$ progression (Figs. 2, 3, and 4) (Table 2).

### The 481, 443, and 223 $cm^{-1}$ bands

Bands at 481 and 223 $cm^{-1}$, along with the progressions of the 481 $cm^{-1}$ band appear in four of the five lazurite spectra and in one of the two haüyne spectra collected with the 405 nm excitation (Figs. 2 and 3; Table 2). In addition, a band at 443 $cm^{-1}$ is visible in the spectrum of lazurite from Brazil (Fig. 2; Table 2). These bands are absent in spectra of ultramarine blues (Fig. 4). This observation is consistent with earlier studies in which no ~480 $cm^{-1}$ band was observed in spectra of synthetic pigments collected with a 405 nm laser (Del Federico et al. 2006). The 481 $cm^{-1}$ band has already been reported in spectra of lazurite and haüyne collected with a 458 nm excitation but was absent in spectra collected with a 532 nm laser and has not been assigned to any species (Caggiani et al. 2014). These previous observations are consistent with ours and suggest that another chromophore species with an absorption maximum in/near the 400–450 nm region is responsible for the 481 and 223 $cm^{-1}$ bands. In all lazurite samples, upon subsequent spectra acquisitions from the same irradiated volume, the 481 and 223 $cm^{-1}$ bands and the progression of the 481 $cm^{-1}$ band rapidly lose intensity (Figs. 5 and 6). Simultaneously, the area of $\nu_1(S_2^-)$ band and its progression gradually increases (Figs. 5 and 6). The breakdown of the 481 and 223 $cm^{-1}$ bands can be further accelerated with increasing laser power as shown in time profiles employing filters that reduce the maximum power to 5, 10, 25, and 50% (Fig. 7).

Our observations indicate a laser-induced reaction of a S-bearing species to $S_2^-$. Indeed, visible light of suitable wavelengths can lead to the breakage of S-S bonds in polysulfur compounds (Steudel and Chivers 2019). The S-bearing species in question has its strongest Raman bands at 481 and 223 $cm^{-1}$, an absorption maximum in/near the 400–450 nm region, must contain at least three sulfur atoms to exhibit two Raman bands and must not contain more than six sulfur atoms to fit the sodalite (β) cages of lazurite and haüyne. The $S_4^{2-}$ polysulfide ion fulfills all these criteria: its $\nu_1$ symmetric S-S stretching vibration is at 480 $cm^{-1}$ (Janz et al. 1976; Chivers and Lau 1982), its absorption maximum is at ~420–430 nm (Martin et al. 1973; Badoz-Lambling et al. 1976) and is small enough to be accommodated in the β cages. Furthermore, the Raman-active

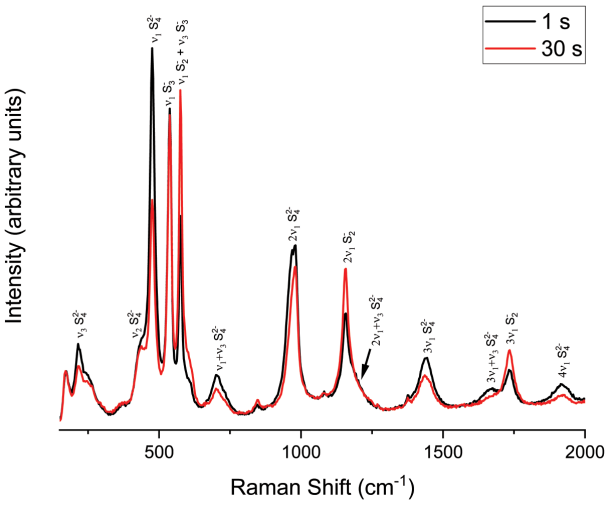


► **Figure 5.** Spectra showing the laser-induced decomposition of the $S_4^{2-}$ polysulfide ions into $S_2$ radicals in lazurite sample NHMG425.086 from Brazil. Both spectra were collected with 405 nm excitation, 50% laser power filter, and for a duration of 1 s. The red spectrum was collected following a 29 s exposure of sample to laser beam, resulting in 30 s of total exposure time.

vibrational frequencies calculated by Tossell (2012) at the cc-pvTZ CCSD PCM level for $S_4^{2-}$ (482 $cm^{-1}$ for the strongest, 228, 449, and 504 $cm^{-1}$) are in close agreement with those observed by us. The laser-induced decomposition of $S_4^{2-}$ likely produces $S_2^-$ according to the reaction:

$$S_4^{2-} \rightarrow 2S_2^-.$$

Indeed, the dissociation of polysulfides to sulfur radicals upon heating or the dimerization of sulfur radicals upon cooling has been observed previously in dissolution experiments of alkali polysulfides (Giggenbach 1968; Seel et al. 1977). Moreover,

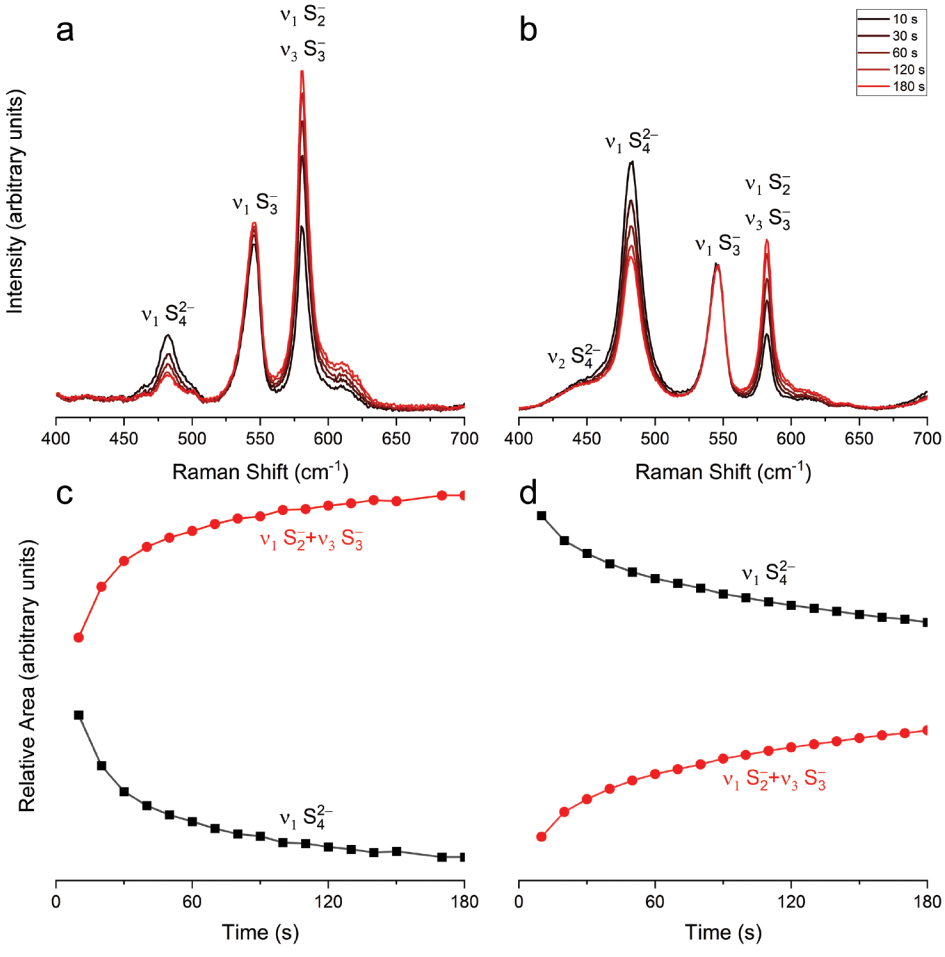


**Figure 6.** (**a** and **b**) Time profiles showing the gradual, laser-induced decomposition of the $S_4^{2-}$ polysulfide ions into $S_2^-$ radicals in lazurite samples. All spectra were collected with the 405 nm excitation, 10% laser power filter, and for a duration of 10 s. The numbers in the key indicate total exposure times to laser beam. (**a**) Sample NHMG003.084 from Baikal, Russia; (**b**) sample NHMG425.086 from Brazil. Note the difference in initial $\nu_1(S_4^{2-})/\nu_1(S_2^-)$ band ratios. (**c** and **d**) Corresponding changes in peak areas.

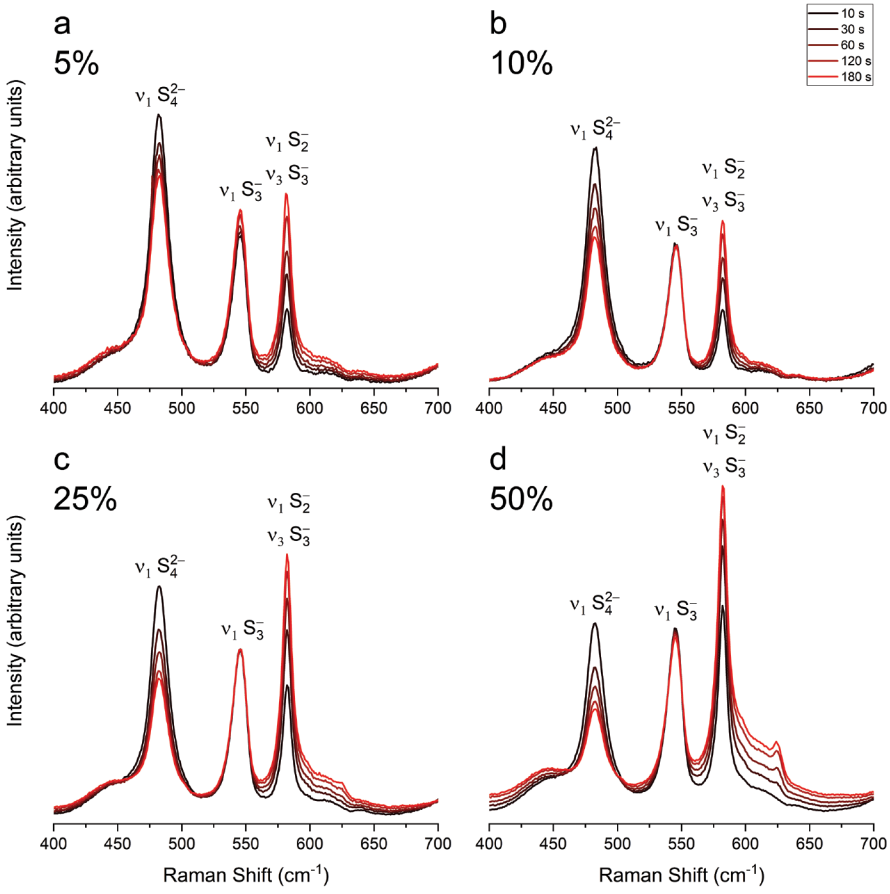


**Figure 7.** Time profiles showing the effect of laser power expressed as a percentage of maximum power (30 mW at the sample) on the gradual, laser-induced decomposition of the $S_4^{2-}$ polysulfide ions into $S_2$ radicals in the NHMG425.086 lazurite sample from Brazil collected with the 405 nm excitation and for a duration of 10 s. The numbers in the key indicate total exposure times to laser beam.

$S_4^{2-}$ has already been successfully trapped in synthetic sodalite structure materials (Ruivo et al. 2018; Lim et al. 2018). Finally, $S_4^{2-}$ has been suggested as a species contributing to an envelope of peaks between 2470 and 2475 eV in the XANES spectra of lazurite (Gambardella et al. 2016). In contrast to lazurite, the $\nu_1$ band of $S_4^{2-}$ in haüyne is only slightly affected by the laser beam, even when using full laser power (Fig. 8). Moreover, there is no growth of the $\nu_1$ band of $S_2^-$ observed that would indicate the decomposition of $S_4^{2-}$. $S_4^{2-}$ is, therefore, much more stable in haüyne than lazurite.

### Ab initio molecular dynamics

To confirm the nature and stability of the radical and polysulfide ions trapped in the sodalite (β) cages of lazurite, we ran a series of ab initio molecular dynamics simulations at 300 K. Lazurite host minerals were modeled using a cubic model host with $[Na_8Al_6Si_6O_{24}]^{2+}$ stoichiometry within either one unit cell or a 2 × 2 × 2 supercell. The $S_3^{2-}$, $S_4^{2-}$, and $S_6^{2-}$ polysulfide groups were placed inside the large cages of the model lazurite in linear geometry parallel to the diagonals of the cube. Using the first minimum of the PDFs (Fig. 9) as the criterion for bonding, the simulations show the large, remarkable stability of the $S_3^{2-}$ linear

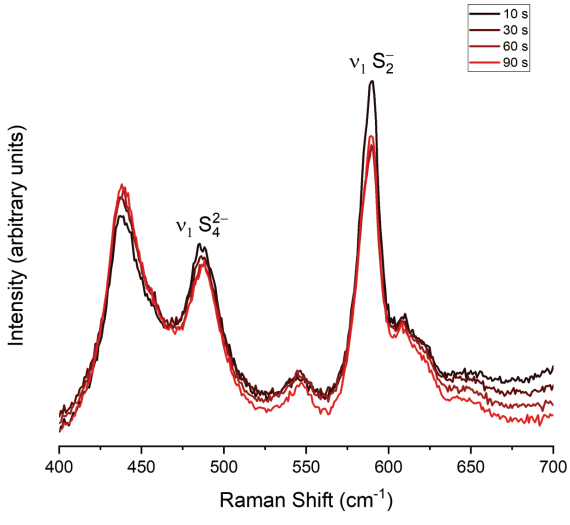


**Figure 8.** Time profile showing the stability of $S_4^{2-}$ polysulfide ions in the NHMG333.049 haüyne sample from Mount Vesuvius, Italy. All spectra were collected with the 405 nm excitation, at full laser power, and for a duration of 10 s. The numbers in the key indicate total exposure times to laser beam.

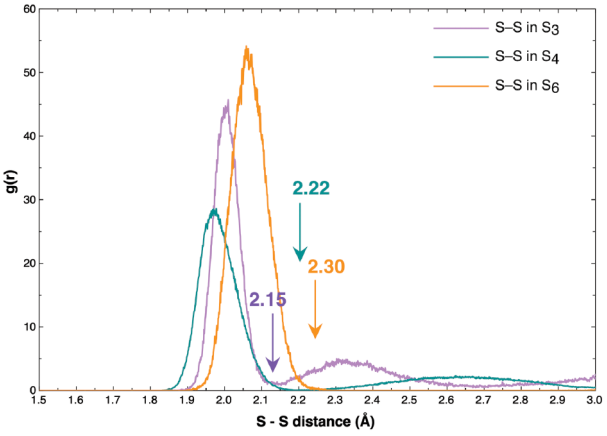


**Figure 9.** S-S pair distribution functions computed for the polysulfide groups trapped in lazurite. The first peak corresponds to the average interatomic bond distance. The first minima (which are marked on the plot) correspond to the radius of the first coordination sphere. Atoms are considered bonded if their distance is less than this radius.

group. In the $S_3^{2-}$ bearing cells, the linear group dominates the sulfur speciation by up to 80%, and the rest of the time, it is split into an $S_2$ group and one isolated S atom. But the lifetime of the isolated $S_2$ + S configuration is <30 femtoseconds. In the $S_4^{2-}$ bearing cells, the complete linear group represents about 6% of the total sulfur population, and the rest of the time, it is split into two $S_2$ molecules. Finally, the $S_6^{2-}$ polysulfide group is split into two $S_3$ linear groups for the entire duration of the simulation. The vibrational analysis reveals peaks corresponding to the $S_2$ and $S_3$ groups, but fails to find any peak corresponding to the $S_4^{2-}$ peak. This is due to the low concentration of the $S_4$ linear group, which is not enough to leave a signature in the total vibrational spectrum. The actual positions of the $S_2$ and $S_3$ peaks are highly dependent on the density of the simulated material, and they appear shifted with respect to experiments. Only the relative $S_2/S_3$ positions are consistent with the experiments.

Simulations that started with tetrahedral $S_4^{2-}$ groups saw their immediate dissociation in two $S_2^-$ molecules. The same phenomenon appeared in simulations of $Na_2S_4$ or $CaS_4$. Moreover, if the density of these systems is too low, the DFT simulations tend to dissociate the molecules and transform them into an amorphous phase, similar to a gas.

### Geometry of the $S_4^{2-}$ polysulfide ion and the assignment of observed bands

The $S_4^{2-}$ polysulfide ion may exist in several geometries, including chain (Tegman 1973), ring (Mealli et al. 2008; Poduska et al. 2009), and branched geometry (Lim et al. 2018). An example of a chain geometry is solid $Na_2S_4$ (Tegman 1973) that has two symmetric stretching modes: a $\nu_1$ symmetric S-S stretching vibration involving a terminal S atom at 482 $cm^{-1}$ and a $\nu_2$ symmetric S-S stretching vibration involving two central S atoms at 445 $cm^{-1}$ (Janz et al. 1976). While in the lazurite from Brazil, there is a prominent shoulder present at ~443 $cm^{-1}$ that may be associated with the $\nu_2$ symmetric S-S stretching vibration; no ~445 $cm^{-1}$ shoulder is present in the lazurite from Russia (Fig. 6). The absence of the $\nu_2$ symmetric S-S stretching vibration in the lazurite from Russia may indicate the presence of $S_4^{2-}$ rings rather than linear $S_4^{2-}$ units, in which all S-S bonds are equivalent leading to only one symmetric S-S stretching vibration. The MD simulation indicates the preference of $S_4^{2-}$ to form linear units rather than rings, and therefore, we propose a chain geometry of $S_4^{2-}$ polysulfide ion in the cage and follow the assignment of vibrational modes proposed by Janz et al. (1976) (Table 2). However, we do not discard the possibility of the existence of $S_4^{2-}$ rings in the sodalite (β) cages of lazurite and haüyne.

### Other S-bearing species

Several additional bands appear in the 230–280 and 600–650 $cm^{-1}$ regions of certain lazurite and haüyne spectra that may be associated with other S-bearing species. However, the assignment of these is not trivial and is beyond the scope of this study.

## Implications

The spectral features of the $S_4^{2-}$ polysulfide ion are only visible in Raman resonance spectra collected with 405 nm excitation that lies inside the absorbance band of $S_4^{2-}$. The absence of these peaks in the MD simulations and in the observations with other laser wavelengths suggests a strong Raman resonance effect. This underlines that Raman resonance spectroscopy a powerful method to detect very low concentrations of $S_4^{2-}$ (and other polysulfides), which are below the detection limit of Raman spectra collected with different excitations or other conventional analytical techniques (e.g., X-ray powder diffraction).

The intensity of the Raman bands of $S_2^-$ and $S_3^-$ radicals is also very strongly enhanced when these species are measured with excitations that lie inside their respective absorption bands, showing that resonance Raman spectroscopy is a powerful qualitative tool to detect very small amounts of sulfur radicals. However, in studies aiming to measure the concentration of sulfur radicals in solutions, Raman resonance should be eliminated, and the quantification of sulfur radicals should only be attempted with excitations lying outside their respective absorption bands (Schmidt and Seward 2017). This is critically important for studies aiming to quantify sulfur radical species in high-pressure-temperature fluids resembling geologic fluids and assess their role in metal mobilization, transport, and ore deposit formation.

Hackmanite, a variety of sodalite, has been suggested to contain $S_2^-$ radicals (Müller 2017). To confirm this suggestion and to detect polysulfide species in different minerals and materials, resonance Raman spectroscopy seems to be the ideal analytical technique.

The laser-induced decomposition of the $S_4^{2-}$ polysulfide ion into two $S_2^-$ radicals in lazurite was observed even while using a 5% laser power filter (corresponding to ~1.5 mW at the sample). Sulfur species are known for their sensitivity to visible light and high probability of beam damage (Steudel and Chivers 2019). Checks for laser-induced reactions and damage and the use of low laser power are therefore recommended when analyzing polysulfides.

Given the post-entrapment and post-cooling immobility of most sulfur species in the sodalite cages of lazurite and

haüyne, their ratios can potentially reflect the chemical state of metasomatizing fluids (Tauson et al. 2011). The distinct $SO_4^{2-}/(S_2^{-}+S_4^{2-})/S_3^{-}$ ratios of the analyzed lazurite samples may also provide hints on the provenance of lazurite used to make ultramarine blue pigments.

Finally, there is considerable interest in entrapping $S_4^{2-}$ into synthetic sodalite structure materials because these show high external quantum efficiency values, large Stokes shifts, and thermal stability and can find applications in light down-conversion systems or as phosphors in lighting devices (Ruivo et al. 2018). $S_4^{2-}$ in haüyne was found surprisingly stable in comparison with lazurite, making haüyne a potentially interesting host material for $S_4^{2-}$ entrapment.

## Acknowledgments

Edwin Gnos from the Natural History Museum of Geneva is acknowledged for lending the lapis lazuli and haüyne samples. We thank Thomas Bürgi from University of Geneva for letting us use his diffuse reflectance spectroscopy setup. Arnulf Rosspeintner and Jafar Afshani from University of Geneva are acknowledged for their assistance with diffuse reflectance measurements. We thank the anonymous reviewers and the associate editor Jianwei Wang for their helpful comments and suggestions.

## Funding

S.F. and Z.Z. acknowledge the European Union because this project was funded by the European Research Council (ERC) under the European Union's Horizon 2020 research and innovation programme (grant agreement no. 864792, ERC Consolidator Grant OXYGEN to Z.Z.). R.C. acknowledges support from the European Research Council (ERC) under the European Union's Horizon 2020 research and innovation programme (grant agreement no. 681818, IMPACT to R.C.), the Research Council of Norway, project number 223272 and through project HIDDEN 325567, and access to supercomputing facilities via the eDARI stl2816 grants, the PRACE RA4947 and RA240046 grant, and the Uninet2 NN9697K grant.

## References cited

Badoz-Lambling, J., Bonnaterre, R., Cauquis, G., Delamar, M., and Demange, G. (1976) La reduction du soufre en milieu organique. Electrochimica Acta, 21, 119–131, https://doi.org/10.1016/0013-4686(76)85048-7.

Blöchl, P.E. (1994) Projector augmented-wave method. Physical Review B: Condensed Matter, 50, 17953–17979, https://doi.org/10.1103/PhysRevB.50.17953.

Caggiani, M.C., Acquafredda, P., Colomban, P., and Mangone, A. (2014) The source of blue colour of archaeological glass and glazes: The Raman spectroscopy/SEM-EDS answers. Journal of Raman Spectroscopy, 45, 1251–1259, https://doi.org/10.1002/jrs.4492.

Caggiani, M.C., Mangone, A., and Acquafredda, P. (2022) Blue coloured haüyne from Mt. Vulture (Italy) volcanic rocks: SEM-EDS and Raman investigation of natural and heated crystals. Journal of Raman Spectroscopy, 53, 956–968, https://doi.org/10.1002/jrs.6310.

Caracas, R., Kobsch, A., Solomatova, N.V., Li, Z., Soubiran, F., and Hernandez, J.A. (2021a) Analyzing melts and fluids from Ab initio molecular dynamics simulations with the UMD package. Journal of Visualized Experiments, 2021, 1–20.

Caracas, R., Kobsch, A., Solomatova, N.V., Li, Z., Soubiran, F., and Hernandez, J.A. (2021b) Analyzing melts and fluids from Ab initio molecular dynamics simulations with the UMD package. Journal of Visualized Experiments, 2021.

Chivers, T. (1974) Ubiquitous trisulphur radical ion $S_3^{-}$. Nature, 252, 32–33, https://doi.org/10.1038/252032a0.

Chivers, T. and Drummond, I. (1972) Characterization of the trisulfur radical anion $S_3^{-}$ in blue solutions of alkali polysulfides in hexamethylphosphoramide. Inorganic Chemistry, 11, 2525–2527, https://doi.org/10.1021/ic50116a047.

Chivers, T. and Lau, C. (1982) Raman spectroscopic identification of the $S_4N^{-}$ and $S_3^{-}$ ions in blue solutions of sulfur in liquid ammonia. Inorganic Chemistry, 21, 453–455, https://doi.org/10.1021/ic00131a089.

Choi, B.-K. and Lockwood, D. (1989) Raman spectrum of $Na_2SO_4$ (Phase V). Solid State Communications, 72, 133–137, https://doi.org/10.1016/0038-1098(89)90893-4.

Clark, R.J.H. and Cobbold, D.G. (1978) Characterization of sulfur radical anions in solutions of alkali polysulfides in dimethylformamide and hexamethylphosphoramide and in the solid state in ultramarine blue, green, and red. Inorganic Chemistry, 17, 3169–3174, https://doi.org/10.1021/ic50189a042.

Clark, R.J.H. and Dines, T.J. (1986) Resonance Raman spectroscopy, and its application to inorganic chemistry. Angewandte Chemie, 25, 131–158, https://doi.org/10.1002/anie.198601311.

Clark, R.J.H. and Franks, M.L. (1975) The resonance Raman spectrum of ultramarine blue. Chemical Physics Letters, 34, 69–72, https://doi.org/10.1016/0009-2614(75)80202-8.

Del Federico, E., Shöfberger, W., Schelvis, J., Kapetanaki, S., Tyne, L., and Jerschow, A. (2006) Insight into framework destruction in ultramarine pigments. Inorganic Chemistry, 45, 1270–1276, https://doi.org/10.1021/ic050903z.

Fleet, M.E., Liu, X., Harmer, S.L., and Nesbitt, H.W. (2005) Chemical state of sulfur in natural and synthetic lazurite by S K-edge XANES and X-ray photoelectron spectroscopy. Canadian Mineralogist, 43, 1589–1603, https://doi.org/10.2113/gscanmin.43.5.1589.

Gaetani, M.C., Santamaria, U., and Seccaroni, C. (2004) The use of Egyptian blue and lapis lazuli in the middle ages: The wall paintings of the San Saba church in Rome. Studies in Conservation, 49, 13–22, https://doi.org/10.1179/sic.2004.49.1.13.

Gambardella, A.A., Schmidt Patterson, C.M., Webb, S.M., and Walton, M.S. (2016) Sulfur K-edge XANES of lazurite: Toward determining the provenance of lapis lazuli. Microchemical Journal, 125, 299–307, https://doi.org/10.1016/j.microc.2015.11.030.

Gettens, R.J. (1938) The materials in the wall paintings of Bamiyan, Afghanistan. Technical Studies in the Field of the Fine Arts, 6, 186–193.

Giggenbach, W. (1968) On the nature of the blue solutions of sulfur. Journal of Inorganic and Nuclear Chemistry, 30, 3189–3201, https://doi.org/10.1016/0022-1902(68)80112-5.

González-Cabrera, M., Wieland, K., Eitenberger, E., Bleier, A., Brunnbauer, L., Limbeck, A., Hutter, H., Haisch, C., Lendl, B., Domínguez-Vidal, A., and others. (2022) Multisensor hyperspectral imaging approach for the microchemical analysis of ultramarine blue pigments. Scientific Reports, 12, 707, https://doi.org/10.1038/s41598-021-04597-7.

Hassan, I. and Grundy, H.D. (1991) The crystal structure of hauyne at 293 and 153 K. Canadian Mineralogist, 29, 123–130.

Hassan, I., Peterson, R.C., and Grundy, H.D. (1985) The structure of lazurite, ideally $Na_6Ca_2(Al_6Si_6O_{24})S_2$, a member of the sodalite group. Acta Crystallographica, C41, 827–832, https://doi.org/10.1107/S0108270185005662.

Holzer, W., Murphy, W.F., and Bernstein, H.J. (1969) Raman spectra of negative molecular ions doped in alkali halide crystals. Journal of Molecular Spectroscopy, 32, 13–23, https://doi.org/10.1016/0022-2852(69)90139-8.

——— (1970) Resonance Raman effect and resonance fluorescence in halogen gases. The Journal of Chemical Physics, 52, 399–407, https://doi.org/10.1063/1.1672699.

Janz, G.J., Downey, J.R., Roduner, E., Wasilczyk, G.J., Coutts, J.W., and Eluard, A. (1976) Raman studies of sulfur-containing anions in inorganic polysulfides. Sodium. Inorganic Chemistry, 15, 1759–1763, https://doi.org/10.1021/ic50162a004.

Kresse, G. and Hafner, J. (1993) Ab initio molecular dynamics for liquid metals. Physical Review B: Condensed Matter, 47, 558–561, https://doi.org/10.1103/PhysRevB.47.558.

Kresse, G. and Joubert, D. (1999) From ultrasoft pseudopotentials to the projector augmented-wave method. Physical Review B: Condensed Matter, 59, 1758–1775, https://doi.org/10.1103/PhysRevB.59.1758.

Ledé, B., Demortier, A., Gobeltz-Hautecœur, N., Lelieur, J.P., Picquenard, E., and Duhayon, C. (2007) Observation of the $\nu_3$ Raman band of $S_3^{-}$ inserted into sodalite cages. Journal of Raman Spectroscopy: JRS, 38, 1461–1468, https://doi.org/10.1002/jrs.1795.

Lim, H.S., Heo, N.H., and Seff, K. (2018) Disproportionation of an element in a zeolite. III. Crystal Structure of a high-temperature sulfur sorption complex of zeolite LTA containing two new ions: perthiosulfite, $S_4^{2-}$, and the trisulfur cation, $S_3^{+}$. The Journal of Physical Chemistry C, 122, 28133–28141, https://doi.org/10.1021/acs.jpcc.8b09223.

Linguerri, R., Komiha, N., Fabian, J., and Rosmus, P. (2008) Electronic states of the ultramarine chromophore $S_3^{-}$. Zeitschrift für Physikalische Chemie, 222, 163–176, https://doi.org/10.1524/zpch.2008.222.1.163.

Martin, R.P., Doub, W.H. Jr., Roberts, J.L. Jr., and Sawyer, D.T. (1973) Electrochemical reduction of sulfur in aprotic solvents. Inorganic Chemistry, 12, 1921–1925, https://doi.org/10.1021/ic50126a047.

Mealli, C., Ienco, A., Poduska, A., and Hoffmann, R. (2008) $S_4^{2-}$ rings, disulfides, and sulfides in transition-metal complexes: The subtle interplay of oxidation and structure. Angewandte Chemie, 47, 2864–2868, https://doi.org/10.1002/anie.200705296.

Müller, H. (2017) La fluorite bleuissante de Tignes, Tarentaise, Savoie. Le Règne Minéral, 42–44.

Nafie, L.A., Stein, P., and Peticolas, W.L. (1971) Time ordered diagrams for the resonant Raman effect from molecular vibrations. Chemical Physics Letters, 12, 131–136, https://doi.org/10.1016/0009-2614(71)80633-4.

Ostroumov, M., Fritsch, E., Faulques, E., and Chauvet, O. (2002) Etude spectrometrique de la lazurite du Pamir, Tajikistan. Canadian Mineralogist, 40, 885–893, https://doi.org/10.2113/gscanmin.40.3.885.

Perdew, J.P., Burke, K., and Ernzerhof, M. (1996) Generalized gradient approximation made simple. Physical Review Letters, 77, 3865–3868, https://doi.org/10.1103/PhysRevLett.77.3865.

Picquenard, E., El Jaroudi, O., and Corset, J. (1993) Resonance Raman spectra of the $S_3$ molecule in sulphur vapour. Journal of Raman Spectroscopy: JRS, 24, 11–19, https://doi.org/10.1002/jrs.1250240103.

Poduska, A., Hoffmann, R., Ienco, A., and Mealli, C. (2009) "Half-bonds" in an unusual coordinated $S_4^{2-}$ rectangle. Chemistry, an Asian Journal, 4, 302–313, https://doi.org/10.1002/asia.200800333.

Pokrovski, G.S. and Dubrovinsky, L.S. (2011) The $S_3^-$ ion is stable in geological fluids at elevated temperatures and pressures. Science, 331, 1052–1054, https://doi.org/10.1126/science.1199911.

Reinen, D. and Lindner, G.G. (1999) The nature of the chalcogen colour centres in ultramarine-type solids. Chemical Society Reviews, 28, 75–84, https://doi.org/10.1039/a704920j.

Ruivo, A., Coutino-Gonzalez, E., Santos, M.M., Baekelant, W., Fron, E., Roeffaers, M.B.J., Pina, F., Hofkens, J., and Laia, C.A.T. (2018) Highly Photoluminescent sulfide clusters confined in zeolites. The Journal of Physical Chemistry C, 122, 14761–14770, https://doi.org/10.1021/acs.jpcc.8b01247.

Sapozhnikov, A.N., Tauson, V.L., Lipko, S.V., Shendrik, R.Y., Levitskii, V.I., Suvorova, L.F., Chukanov, N.V., and Vigasina, M.F. (2021) On the crystal chemistry of sulfur-rich lazurite, ideally $Na_7Ca(Al_6Si_6O_{24})(SO_4)(S_3)\cdot nH_2O$. American Mineralogist, 106, 226–234, https://doi.org/10.2138/am-2020-7317.

Schmidt, C. and Seward, T.M. (2017) Raman spectroscopic quantification of sulfur species in aqueous fluids: Ratios of relative molar scattering factors of Raman bands of $H_2S$, $HS^-$, $SO_2$, $HSO_4^-$, $SO_4^{2-}$, $S_2O_3^{2-}$, $S_3^-$ and $H_2O$ at ambient conditions and information on changes with pressure and tempe. Chemical Geology, 467, 64–75, https://doi.org/10.1016/j.chemgeo.2017.07.022.

Seel, F., Güttler, H.-J., Simon, G., and Wieckowski, A. (1977) Colored sulfur species in EPD-solvents. Pure and Applied Chemistry, 49, 45–54, https://doi.org/10.1351/pac197749010045.

Shnitko, I., Fulara, J., Garkusha, I., Nagy, A., and Maier, J.P. (2008) Electronic transitions of $S_2^-$ and $S_3^-$ in neon matrixes. Chemical Physics, 346, 8–12, https://doi.org/10.1016/j.chemphys.2008.01.005.

Steudel, R. and Chivers, T. (2019) The role of polysulfide dianions and radical anions in the chemical, physical and biological sciences, including sulfur-based batteries. Chemical Society Reviews, 48, 3279–3319, https://doi.org/10.1039/C8CS00826D.

Tauson, V.L., Sapozhnikov, A.N., Shinkareva, S.N., and Lustenberg, E.E. (2011) Indicative properties of lazurite as a member of clathrasil mineral family. Doklady Earth Sciences, 441, 1732–1737, https://doi.org/10.1134/S1028334X11120312.

Tauson, V.L., Goettlicher, J., Sapozhnikov, A.N., Mangold, S., and Lustenberg, E.E. (2012) Sulphur speciation in lazurite-type minerals $(Na,Ca)_8[Al_6Si_6O_{24}](SO_4,S)_2$ and their annealing products: A comparative XPS and XAS study. European Journal of Mineralogy, 24, 133–152, https://doi.org/10.1127/0935-1221/2011/0023-2132.

Tegman, R. (1973) The crystal structure of sodium tetrasulphide, $Na_2S_4$. Acta Crystallographica, B29, 1463–1469, https://doi.org/10.1107/S0567740873004735.

Tossell, J.A. (2012) Calculation of the properties of the $S_3^-$ radical anion and its complexes with $Cu^+$ in aqueous solution. Geochimica et Cosmochimica Acta, 95, 79–92, https://doi.org/10.1016/j.gca.2012.07.020.

Manuscript received June 15, 2022
Manuscript accepted May 11, 2023
Accepted manuscript online May 18, 2023
Manuscript handled by Jianwei Wang

## Endnote:

[1]Deposit item AM-23-128655. Online Materials are free to all readers. Go online, via the table of contents or article view, and find the tab or link for supplemental materials.